Preparation and Characterization of Fe₂O₃-CaO-SiO₂ Porous Glass Ceramics for Bacteria Immobilization

Bin LI [1], Yong Ya WANG [2] *, Wen Qin LUO [2]

[1] *School of Life Science, Huzhou University, Huzhou 313000, China*
[2] *Department of Material Chemistry, Huzhou University, Huzhou 313000, China*

In this work we present a study of porous glass ceramics towards bacteria-immobilization applications for water filtration. Sol-gel synthesized glass samples were processed into Fe₂O₃-CaO-SiO₂ porous glass ceramics by introducing a pore forming agent. The crystal phase composition, morphology, and pore structure of the ceramics were characterized by X-ray diffraction (XRD), scanning electron microscopy (SEM), N2 adsorption-desorption measurements, and mercury intrusion porosimetry. By varying the pore forming agent and process conditions, varied pore size distributions are produced. The volume fraction of macropores is overall large while the volume fraction of meso-pores and micropores is overall comparably small. All samples display good biocompatability and compressive strength, making them suitable for bacteria immobilization. The macropore sizes were determined primarily by the size of pore forming agent, enabling control. The results provide a basis for optimizing the preparation of porous glass ceramics for bacteria immobilization.
Keywords: porous glass ceramics, sol-gel, pore forming agent.

1. INTRODUCTION

Ammonia treatment is crucial in wastewater management. Traditional processes for the treatment of ammonia nitrogen however have many disadvantages, including high cost, high energy consumption, and low efficacy [1]. Biological treatments, using nitrifying bacteria to eliminate ammonia nitrogen, were demonstrated to be superior in both efficiency and efficacy [2, 3], leading to their wide adoption. Lingering deficiencies in the most popular bacterial treatments can be overcome by immobilizing the nitrifying bacteria, a blossoming area of research [4, 5]. Choosing an appropriate immobilized carrier is critical to the success of this technology [6 – 8]. Porous inorganic materials in particular have attracted recent interest as carriers because of their large surface area and biocompatibility [9, 10]. D. Jiang *et al.* studied the adsorption mechanism of Pseudomonas putida on clay [11]. L.L. Liu *et al.* explored immobilized sorangium cellulosum on a diatomite-based porous ceramic [12]. The water-processing activity of microbes immobilized on porous inorganic materials has also been studied [13, 14].

Porous glass ceramics are an especially attractive potential candidate material, with a large specific surface area and high concentration of internal active cations [15, 16]. To date however, only the adsorption of gas and metal ions in these materials has been studied [17, 18]; the microbial immobilization mechanism has yet to be investigated [19 – 21].

In this work, we present the preparation of porous glass ceramics that could be used for bacteria immobilization. Because pore structure can play a significant role in bacteria immobilization, a series of pore sizes in such glass ceramics must be studied. To do so, we first prepared a glass powder via sol-gel method. Then, porous glass ceramics with a controlled pore size distribution were prepared by adding pore forming agent. The physical properties, crystal phase, morphology, and pore structure of the porous glass ceramics were analyzed. These results enable optimization of the preparation process of porous glass ceramics in their application to bacteria immobilization.

2. EXPERIMENTAL DETAILS

2.1. Preparation of Fe₂O₃-CaO-SiO₂ porous glass ceramics

Fe₂O₃-CaO-SiO₂ glass samples (Fe₂O₃ 15 wt.%, CaO 42 wt.%, SiO₂ 43 wt.%) were prepared via sol-gel synthesis [22]. These glass samples were ground into a powder and mixed with a pore forming agent and polyvinyl alcohol binder. The pore forming agent of sample 21010 and B11020 was sodium bicarbonate while the pore forming agent of sample S2A4 was bamboo powder. The pore forming agent of sample 21010 was sieved through a 100-mesh gauze and that of B11020 was sieved through a 150-mesh gauze. The samples were then pressed into strips at varying pressures with a tablet press (Table 1), followed by further sintering in air by heating at a rate of 5 °C/min to 1050 °C and holding for 1 h.

Table 1. Preparation conditions of different samples

Sample	Glass, wt.%	Pore forming agent, wt.%	Polyvinyl alcohol, wt.%	Pressure, MPa
21010	85	10	5	10
B11020	85	10	5	20
S2A4	85	10	5	20

---

* Corresponding author. Tel.: +86-0572-2599685; fax: +86-0572-2599806. E-mail address: *arince@zjhu.edu.cn* (Y.Y. Wang)

2.2. Characterization

The water absorption and apparent porosity of the samples were determined using the vacuum method. First, the sample was cleaned and dried in an over, then cooled to room temperature. The weight of the sample is m_1. Next, the samples were placed in a beaker and vacuum dried at 0.133 kPa for 5 min. Distilled water was slowly injected into the beaker until the samples were immersed for 5 min, and the sample together with the container were removed from the vacuum oven. Then, the saturated sample was placed in a wire basket and suspended in a water container. The saturated sample weight in liquid is m_2. Finally, the saturated sample was removed from the liquid and quickly wiped to remove the water attached to the surface. The saturated sample weight in air is m_3. The water absorption and apparent porosity of the samples were calculated using to the following equations, water absorption:

$$W_a = \frac{m_3 - m_1}{m_1} \times 100\% \text{ ,} \tag{1}$$

and apparent porosity:

$$P_a = \frac{m_3 - m_1}{m_3 - m_2} \times 100\% \text{ .} \tag{2}$$

Compressive strength was tested using an electronic universal testing machine (WDW-H10) following the standard test method for ceramic material compressive resistance (China, GB/T 4740-1999).

X-ray diffraction (XRD) analysis was performed with an XD-6 X-ray diffractometer at room temperature, with CuKα radiation, 36 kV voltage and 20 mA current. X-ray data were collected in the $5° < 2θ < 80°$ range.

The microstructures of the samples were observed using scanning electron microscopy (SEM) (S-3400N). To improve imaging, the samples were coated with an approximately 10 nm thick layer of Au.

The adsorption-desorption isotherms of samples were determined by a ASAP 2020 nitrogen adsorption-desorption apparatus. The specific surface area and pore size distribution of the sample were calculated with a Brunauer-Emmett-Teller (BET) model. The sample was heated to 250 °C and degassed for 6 h at 200 °C before the test.

The macroscopic pore size distributions of the samples were analyzed using mercury intrusion porosimetry (IV AutoPore 9510, USA) at room temperature.

Cytotoxicity of porous glass ceramics samples B11020 to FHC cells (CRL-1831[TM]) was detected using a cell counting kit-8 (CCK-8). FHC cells in logarithmic growth phase were plated (5×10^4 cells/well) in 96-well plates and cultured in an atmosphere of 5 % CO_2 at 37 °C. Then, 10 % fetal bovine serum (FBS, Gibco), penicillin (l00 U/mL), and streptomycin (100 µg/mL) were added to the culture medium. The supernatant was removed after 48 h of culture. The cell culture medium was replaced by a culture medium with porous glass ceramics samples (0 µg/mL, 6 µg/mL, 12.5 µg/mL, 25 µg/mL, 50 µg/mL, 100 µg/mL, 200 µg/mL) and cultured for 24 h. Then the supernatant was removed and the wells of culture plates were rinsed twice with phosphate buffered saline (PBS). Each well was replaced with 100 µl fresh complete culture medium. 10 µl CCK-8 solution was added to the well, and cultured for an additional 2 hours. Finally, the well absorbance was measured at 450 nm using a microplate reader (Thermo) to determine the cell survival rate. Each independent experiment was performed in quadruplicate. The control wells were assayed as blank controls and subtracted from the corresponding specimens. Data are expressed as mean values and standard deviations for each sample group.

3. RESULTS AND DISCUSSION

3.1. Physical properties of porous glass ceramic samples

The physical properties of the porous glass ceramic samples, as determined by the vacuum method and an electronic universal testing machine, are listed in Table 2. Apparent porosities of all the samples are over 30 %, indicating that the samples are of moderate porosity. The apparent porosity and water absorption rate of sample S2A4 is the highest of all the samples, but the compressive strength is only 4 MPa, limiting the range of feasible application for the material. The lower compressive strength of sample S2A4 was due to its higher apparent porosity and larger grain size, which will be shown in the following sections. Sample 21010 displays both a significant apparent porosity and reasonable compressive strength, making it suitable for bacteria immobilization. The higher porosity is favorable for the growth of bacteria while the larger compressive strength can resist the pressure of the water and thus plays a role in protecting the bacteria.

Table 2. Physical properties of porous glass ceramic samples

Sample	Water absorption, %	Apparent porosity, %	Volume density	Compressive strength, MPa	Elastic modulus, MPa
21010	19.6	35	1.777	16	703
B11020	16.8	33.7	2.003	304	5555
S2A4	38.9	53.8	1.379	4	294

3.2. Surface morphology and crystal phase

SEM images of the samples are reproduced in Fig. 1. Both macro- and micro-pores exist in all samples. The surface of sample 21010 and B11020 display a more uniform pore distribution. The samples have smooth surfaces and compact structures. Sample S2A4 has a loose structure, bigger particle size, and uneven surface, possibly explaining its lower compressive strength. The capillary force between particles is the main factor influencing strength during sintering process, densifying the material [23]. The bamboo powder produces small particles with high plasticity, reducing the capillary force.

XRD patterns of the porous glass ceramic samples are shown in Fig. 2, demonstrating the presence of a mixture of crystalline phases for all the samples. Two major crystalline phases, wollastonite (JCPDS No. 84-0654) and hematite (JCPDS No.85-0599) were observed in sample 21010 and B11020. In addition to those phases, the XRD pattern of sample S2A4 was characterized by the appearance of a significant pseudo-wollastonite phase

(JCPDS No. 74-0874). This is mainly due to the use of bamboo powder as the pore forming agent.
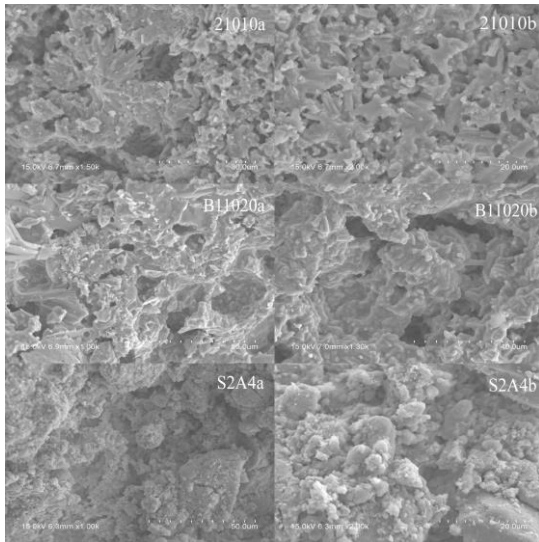

Fig. 1. Scanning electron microscope (SEM) images of porous glass ceramic samples
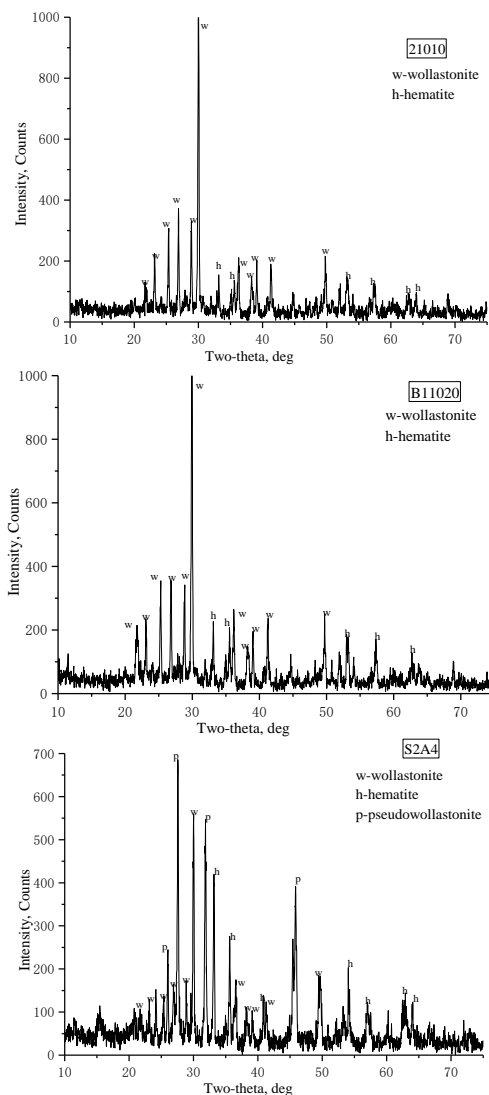

Fig. 2. Room temperature XRD patterns of porous glass ceramic samples

The bamboo powder ash plays the role of flux in the sintering process, which could reduce the formation temperature of pseudo-wollastonite. Glass ceramics with the above crystal phases are biocompatible, making these sample feasible carriers [24], because the hydrated silica formed on the surface of wollastonite and pseudo-wollastonite provides favorable sites for apatite nucleation.

3.3. Cytotoxicity analysis

The activity of FHC cells cultured with different content porous glass ceramics samples are shown in Fig. 3. The FHC cell activities in all the experimental groups were over 80 % after the introduction of porous glass ceramics samples. The FHC cell activity in the 100 µg/ml experimental group was the lowest, while the FHC cell activity in the 12.5 µg/ml experimental group was the highest. The cell survival rate in the experimental group did not change significantly compared to the blank group. The absorbance of each group with different content porous glass ceramics samples showed a significant difference ($p < 0.05$, t-Student test) compared to the blank group, which shows that the experimental group had more advantages in promoting cell proliferation. The results demonstrate that the porous glass ceramics samples present a small cytotoxic potential; there was no obvious inhibition of FHC cell proliferation in this period. Similarly, Ferraz et al. observed that a particulated bioactive ceramic did not promote any cytotoxic effects in cultures of human osteosarcoma cells [25]. Other biocompatible porous glass samples have been observed in previous research [26, 27], so porous glass ceramics samples could be used for bacterial immobilization.
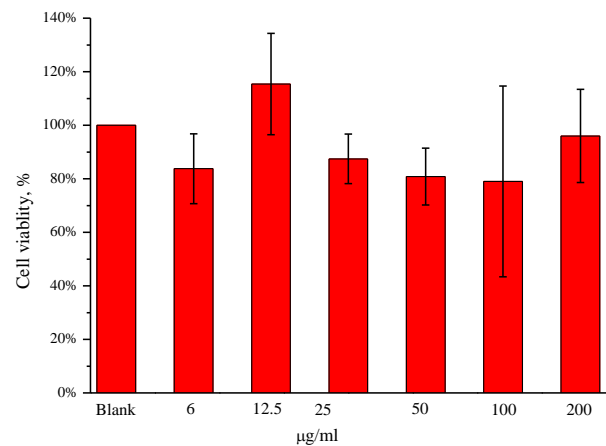

Fig. 3. The FHC cell activity cultured with different sample B11020 content

3.4. Pore size sample characteristics

The N2 adsorption-desorption isotherms of sample S2A4 are reproduced in Fig. 4 a. The low pressure side is raised and the high pressure side was downward-concave, indicating that the material belongs to the II isothermal adsorption desorption curve family. That suggests that there may be a high density of large pores in porous lattice. The low pressure is raised, which indicates that the sample has a large number of mesopores and micropores. The first layer adsorption heat was larger than the liquefaction heat of the gas when gas adsorbed in the hole, so the adsorption

energy is larger than gas intermolecular attraction [28]. The high pressure side rises steeply and does not saturate, indicating that the samples contain macropores larger than 50 nm. That finding is consistent with the pore size distribution observed in mercury intrusion below. The adsorption-desorption isotherm curve did not close, showing that the pore diameters are non-uniform and skew large. BJH pore size distributions (Fig. 4 b) show that the pore sizes of the samples are mainly distributed in the mesoporous range. The pore size distribution of S2A4 was unimodal in the range of 30 – 80 nm, with a peak between 25 and 45 nm. The peak diameter of 21010 and B11020 was between 2 and 10 nm, much smaller than that of S2A4.

mercury increasingly injects into meso- and micro-pores with increasing pressures, the injection volume corresponds to the incidence of meso- and micro-pores. The rapid saturation in all samples indicates that the volume of meso- and micro-pores in the samples is relatively low.

Fig. 5. Mercury-injection volume curves of porous glass ceramics samples

The macroporous size distributions calculated from mercury intrusion porosimetry are shown in Fig. 6. The pore size distribution of the porous block is sharp. The macroporous distribution of both 21010 and B11020 are located in the range of 1 – 5 μm. The peak pore size of B11020 is 1.6 μm while the peak pore size of 21010 is 2 μm. The difference could be attributed to the difference in size of the pore forming agents. The macropore distribution of S2A4 appears in the range of 4 – 12 μm, with a peak at 4.5 μm.

Fig. 6. Macroporous size distribution of porous glass ceramics samples

Both BET and mercury intrusion porosimetry show that a series of pore size distributions are produced in the samples. The pore size distributions of the macropores could be controlled by the size of the pore forming agent.
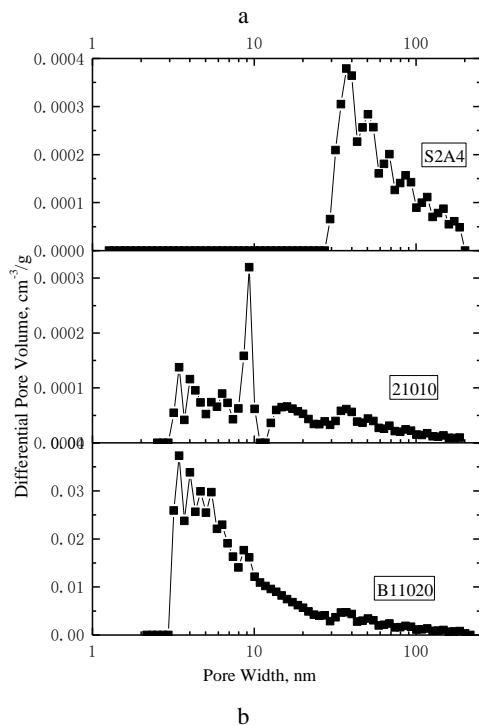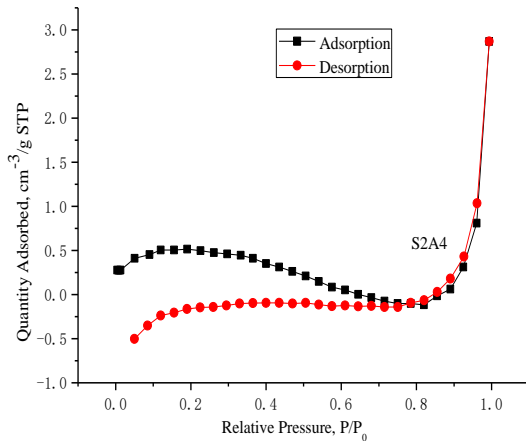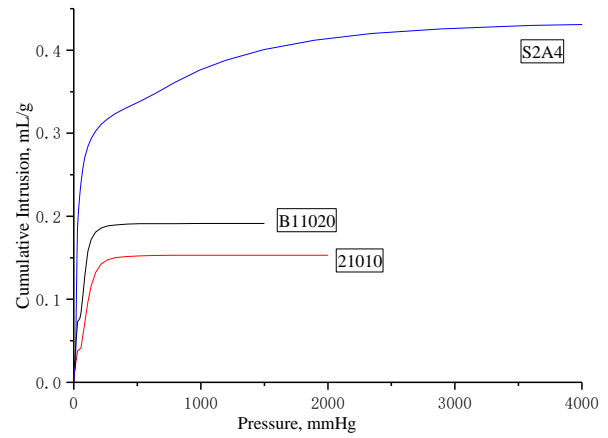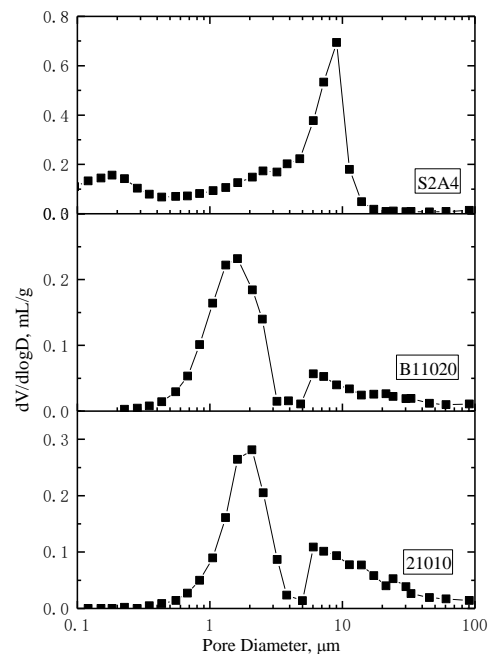

Fig. 4. a – N₂ adsorption-desorption isotherms of S2A4; b – pore size distribution of porous glass ceramics samples

Mercury-injection volume curves of the porous glass ceramics samples are shown in Fig. 5. The mercury injection volume increases rapidly in the low pressure regime before saturating, reflecting the macroporosity of the sample [29]. The mercury injection of S2A4 is the most rapid, confirming the larger pore size distribution. As

The volume fraction of macropores is comparatively large while the volume fraction of the meso-pores and micropores is smaller, a favorable condition for immobilized microorganisms. Macropores can be used for microorganism residence while micro- and mesopores can be used for mass transfer after bacterial enrichment, helping to avoid bacterial death caused by the poor mass transfer due to macropore blockage. This feature is important to extending the survival time of bacteria on the carrier, and is one of the current challenges faced by carrier materials. Further work is in progress in our laboratory to understand the effect of pore size distributions on the immobilization of nitrifying bacteria.

4. CONCLUSIONS

In this work, glass powders were prepared via sol-gel method and porous glass ceramic blocks with various pore size distributions were prepared by introducing a pore forming agent. The results show that the choice of pore forming agent impacts strength and pore size distribution of the resulting porous glass ceramics. We find that Fe_2O_3-CaO-SiO_2 porous glass ceramics are promising carriers of immobilized bacteria. The crystal phase and the pore size distribution are optimal for bacteria immobilization.

REFERENCES

1. **Judd, S.** A Review of Fouling of Membrane Bioreactors in Sewage Treatment *Water Science and Technology* 49 2004: pp. 229 – 235.

2. **Rosala, R., Rodrígueza, A., Perdigón-Melón, J.** Occurrence of Emerging Pollutants in Urban Wastewater and their Removal Through Biological Treatment Followed by Ozonation *Water Research* 44 2010: pp.578 – 588.

3. **Jemli, M., Karray, F., Feki, F.** Biological Treatment of Fish Processing Wastewater: A Case Study From Sfax City (Southeastern Tunisia) *Journal of Environment Science* 30 2015: pp. 102 – 112.
https://doi.org/10.1016/j.jes.2014.11.002

4. **Obbard, J., Shan, H.** Ammonia Removal from Prawn Aquaculture Water Using Immobilized Nitrifying Bacteria *Applied Microbiology and Biotechnology* 57 2001: pp. 791 – 798.

5. **Kariminiaae, H.H., Kanda, K., Kato, F.** Wastewater Treatment with Bacteria Immobilized onto a Ceramic Carrier in an Aerated System *Journal of Bioscience and Bioengineer* 95 2003: pp. 128 – 132.

6. **Silva, A.J., Hirasawa, J.S., Varesche, M.B.** Evaluation of Support Materials for the Immobilization of Sulfate-Reducing Bacteria and Methanogenic Archaea *Anaerobe* 12 2006: pp. 93 – 98.

7. **Ignacio, M.G.** Microalgae Immobilization: Current Techniques and Uses *Bioresource Technology* 99 2008: pp. 3949 – 3964.
https://doi.org/10.1016/j.biortech.2007.05.040

8. **Alvarez, G., Foglia, M., Copello, G.** Effect of Various Parameters on Viability and Growth of Bacteria Immobilized in Sol-Gel-Derived Silica Matrices *Applied Microbiology and Biotechnology* 82 2009: pp. 639 – 646.
https://doi.org/10.1007/s00253-008-1783-9

9. **Rowe, O.F., Johnson, D.B.** Comparison of Ferric Iron Generation by Different Species of Acidophilic Bacteria Immobilized in Packed-Bed Reactors *Systematic & Applied Microbiology* 31 2008: pp. 68 – 77.
https://doi.org/10.1016/j.syapm.2007.09.001

10. **Su, Y., Zhang, Y., Wang, J.** Enhanced Bio-Decolorization of Azo Dyes by Co-Immobilized Quinone-Reducing Consortium and Anthraquinone *Bioresource Technology* 100 2009: pp. 2982 – 2987.

11. **Jiang, D., Huanga, Q., Cai, P.** Adsorption of Pseudomonas Putida on Clay Minerals and Iron Oxide *Colloids and Surfaces B* 54 2007: pp. 217 – 221.

12. **Liu, L.L.** Fermentation Preparation of Epothilone by Sorangium Cellulosum Immobilized by Porous Ceramic, Master thesis, Shaanxi university of science and technology, 2014.

13. **Wu, S.Q., Yue, Q.Y., Qi, Y.F.** Preparation of Ultra-Lightweight Sludge Ceramics (ULSC) and Application for Pharmaceutical Advanced Wastewater Treatment in a Biological Aerobic Filter (BAF) *Bioresource Technology* 102 2011: pp. 2296 – 2300.
https://doi.org/10.1016/j.biortech.2010.10.057

14. **Zou, J.L., Xu, G.R., Pan, K.** Nitrogen Removal and Biofilm Structure Affected by COD/NH^{4+}-N in a Biofilter with Porous Sludge-Ceramsite *Separation and Purification Technology* 94 2012: pp. 9 – 15.
https://doi.org/10.1016/j.seppur.2012.03.019

15. **Tetsuo, Y., Fumiko, M., Kaori, O.** Novel Porous TiO_2 Glass-Ceramics with Highly Photocatalytic Ability *Ceramics International* 35 2009: pp. 1693 – 1697.

16. **Simão, L., Caldato, R.F., Innocentini, M.D.M.** Permeability of Porous Ceramic Based on Calcium Carbonate as Pore Generating Agent *Ceramics International* 41 2015: pp. 4782 – 4788.

17. **Yusuke, D., Hiroki, Y., Toshihiro, K.** Preparation of Porous Titanium Phosphate Glass-Ceramics for NH_3 Gas Adsorption with Self-Cleaning Ability *Journal of the European Ceramic Society* 28 2008: pp. 267 – 270.
https://doi.org/10.1016/j.jeurceramsoc.2007.05.016

18. **Qiu, S., Ma, F., Huang, X., Xu, S.W.** Study on the Adsorption of Bacteria in Ceramsite and their Synergetic Effect on Adsorption of Heavy Metals *Water Science and Technology* 69 2014: pp. 407 – 413.

19. **Hori, K., Matsumoto, S.** Bacterial Adhesion: from Mechanism to Control *Biochemical Engineering Journal* 48 2010: pp. 424 – 434.

20. **Nikolajeva, V., Griba, T., Petriņa, Z.** Factors Influencing Adhesion of Pseudomonas Putida on Porous Clay Ceramic Granules *Environmental and Experimental Biology* 10 2012: pp. 77 – 80.

21. **Sabree, I., Gough, J.E., Derby, B.** Mechanical Properties of Porous Ceramic Scaffolds: Influence of Internal Dimensions *Ceramics International* 41 2015: pp. 8425 – 8432.

22. **Wang, Y.Y., Li, B., Yu, Y.L., Tang, P.S.** Evaluating the

Effects of Chemical Composition on Induction Heating Ability of Fe_2O_3-Cao-Sio_2 Glass Ceramics *Advances in Materials Science & Engineering* 2016 2016: pp. 1 – 7.

23. **Zhang, M.L.** Preparation of Series Porous Ceramic Filter Materials from Waste Solid, Master thesis, Wuhan university of technology, 2008.

24. **Yang, J.K., Yang, S.H., He, G.L., Xiao, B.** The Magnetic Properties And Bioactivity of Ferromagnetic Glass-Ceramics in the System Fe_2O_3-CaO-SiO_2 *Journal of Applied Science* 23 2005: pp. 209 – 213.

25. **Ferraz, M.P., Knowles, J.C., Olsen, I.** Flow Cytometry Analysis of the Effects of Pre-Immersion on the Biocompatibility of Glass-Reinforced Hydroxyapatite Plasma-Sprayed Coatings *Biomaterials* 21 2000: pp. 813 – 820.

26. **Jie, Q., Lin, K.L., Zhong, J.P.** Preparation of Macroporous Sol-Gel Bioglass Using PVA Particles as Pore Former *Journal of Sol-Gel Science and Technology* 30 2004: pp. 49 – 61.

27. **Almeida, R.M., Gama, A., Vueva, Y.** Bioactive Sol-Gel Scaffolds with Dual Porosity for Tissue Engineering *Journal of Sol-Gel Science and Technology* 57 2011: pp. 336 – 342.

28. **Sing, K.S.W.** Adsorption Methods for the Characterization of Porous Materials *Advances in Colloid & Interface Science* 77 1998: pp. 3 – 10.

29. **Li, G.X.** Adsorption Science. Chemical Industry Press, Beijing, 2005: pp. 65 – 72.